Applied Catalysis B: Environmental 140–141 (2013) 16–24

Contents lists available at SciVerse ScienceDirect

Applied Catalysis B: Environmental

journal homepage: www.elsevier.com/locate/apcatb

Hybrid Cu–ZnO–ZrO_2/H-ZSM5 system for the direct synthesis of DME by CO_2 hydrogenation

G. Bonura [a], M. Cordaro [b], L. Spadaro [a], C. Cannilla [a], F. Arena [b], F. Frusteri [a,*]

[a] CNR-ITAE, Institute for Advanced Energy Technologies "Nicola Giordano", Via S. Lucia Sopra Contesse, 5, 98126 Messina, Italy
[b] Department of Industrial Chemistry & Engineering Materials, University of Messina, V.le F. Stagno D'Alcontres 31, 98166 Messina, Italy

ARTICLE INFO

Article history:
Received 11 January 2013
Received in revised form 19 March 2013
Accepted 27 March 2013
Available online 2 April 2013

Keywords:
CO_2 hydrogenation
DME synthesis
Cu–ZnO–ZrO_2 catalysts
Hybrid systems

ABSTRACT

One-step CO_2 hydrogenation reaction to dimethyl ether (DME) was studied on a hybrid system characterized by different reactor bed configurations (physical mixing, dual-bed and mono-bed). Homemade Cu–ZnO–ZrO_2 methanol catalytic system and a commercial H-ZSM5 zeolite were used to realize the hybrid system. The influence of preparation method on activity, selectivity and yield in the temperature range of 453–513 K at 3.0 MPa and $CO_2/H_2/N_2$ feed concentration of 3/9/1 has been evaluated. The results obtained under kinetic conditions show a superior specific productivity of *ca.* 430 $g_{total\ MeOH}\ kg_{cat}^{-1}\ h^{-1}$ at 513 K using the hybrid catalyst prepared by physical mixing. A combined effect of sites located at metal/oxide(s)-acid interface to drive DME synthesis through a consecutive mechanism was claimed as the main factor affecting the CO_2 conversion and DME productivity.

1. Introduction

CO_2 conversion into useful chemicals, like methanol and/or dimethyl ether (DME), is an attractive way to cut down the *greenhouse-gas* emissions, also accomplishing an effective recycle of carbon dioxide [1–5]. Currently, DME is proposed as an alternative clean fuel for diesel engines and household uses, also being a potential hydrogen carrier for fuel cells applications [5–7].

Notwithstanding an extensive literature documents the feasibility of a process for the production of DME *via* syngas [8–19], only few papers deal with the direct (one step) DME synthesis by CO_2 hydrogenation [5,20–29], even if many experiments performed at high contact time and approaching the equilibrium values do not allow to assess a "real" catalytic performance in a full kinetic regime [21,22,28,30–32].

Catalysts for the direct CO_2-to-DME process should be able to efficiently catalyze both the methanol synthesis and the methanol dehydration reactions. This can be accomplished by using bifunctional or hybrid catalysts, typically composed by a Cu–ZnO-based methanol synthesis catalyst [4,5] and a solid acid, like γ-Al_2O_3 [33–37] or H-ZSM5 zeolite [38–46].

Among several catalytic formulations proposed for methanol synthesis, according to previous studies, the Cu–ZnO–ZrO_2 (ZCZ) system [47–50], prepared by "*reverse co-precipitation under ultrasound irradiation*" of catalyst precursors had shown a superior activity compared to conventional catalysts. In particular, the role of metal/oxide(s) interface resulted to be crucial, owing to the interaction of metal Cu particles with both ZnO and ZrO_2 leading to the stabilization of $Cu^{\delta+}$ sites and a "mix" of Cu^0, $Cu^{\delta+}$ and oxide basic sites concurring to the adsorption/activation of H_2, CO and CO_2 [19,47–49].

Besides, as so far reported [34,44,51], H-ZSM5 is more suitable than γ-Al_2O_3 as the dehydration component in bifunctional/hybrid CO_2-to-DME catalysts as the former exhibits much higher activity at moderate reaction temperatures (*ca.* 473–533 K) which are thermodynamically more favourable for the methanol synthesis step [36,51]. Furthermore, water formed by CO_2 hydrogenation and methanol dehydration strongly adsorbs on the Lewis acid sites of γ-Al_2O_3 inhibiting DME formation. By contrast, the effect of water is much less significant for H-ZSM5 owing to its more hydrophobic character and predominance of Brønsted-type acidity [36,44,51]. Still, operation at moderate reaction temperature (<543 K) avoids the need for partially exchanging zeolite, as the inhibition of strong acid sites affecting coke and hydrocarbons formation is not necessary [36].

Therefore, the aim of this work is to investigate the behaviour of a hybrid system constituted by Cu–ZnO–ZrO_2 methanol synthesis catalyst [48–50] and a commercial H-ZSM5 zeolite. The influence of the procedure chosen for the combination of the two active phases on activity, selectivity and productivity of the catalytic system in the direct hydrogenation of CO_2–DME is discussed.

* Corresponding author. Tel.: +39 090624233.
E-mail address: francesco.frusteri@itae.cnr.it (F. Frusteri).

0926-3373/$ – see front matter © 2013 Elsevier B.V. All rights reserved.
http://dx.doi.org/10.1016/j.apcatb.2013.03.048

2. Experimental

2.1. Catalyst preparation

Cu–ZnO–ZrO_2 methanol catalyst (ZCZ) was prepared by "reverse coprecipitation method under ultrasound irradiation", as elsewhere described [50].

A commercial NH_4-ZSM5 zeolite (*CBV 3024E*, Zeolyst International, SiO_2/Al_2O_3 = 30 mol/mol, SA_{BET} = 400 $m^2\,g^{-1}$) was converted in its protonic form (HZ30) by calcination at 773 K in static air for 5 h. All the samples were crushed and sieved and the 40–70 mesh particle size fraction was used for characterization and testing measurements.

Experiments were carried out by charging the reactor with a hybrid system "ZZ", prepared using different combination procedures, as following described:

(a) homogeneous physical mixture, constituted by two pre-pelletized ZCZ and HZ30 catalysts (ZZ-M);
(b) dual-bed composed by a pre-pelletized ZCZ methanol catalyst (first bed) and HZ30 catalyst (second bed) (ZZ-D);
(c) mono-bed constituted by a homogeneous solid mixture, prepared by grinding in an agate mortar of powdered single catalysts and pelletization of the resulting hybrid system (ZZ-G).

2.2. Catalysts characterization

2.2.1. Surface area (SA) and pore volume (PV)

SA and PV values of catalysts were determined from nitrogen adsorption/desorption isotherms at −196 °C, using a *Sorptomatic 1900 Instrument* gas adsorption device. The isotherms were elaborated according to the BET method for surface area calculation, while Horwarth–Kavazoe (HK) and Barrett–Joyner–Halenda (BJH) methods were used for micro- and meso-pores evaluation, respectively.

2.2.2. Temperature programmed reduction (TPR)

The measurements of reducibility in hydrogen atmosphere were performed in a linear quartz micro-reactor (i.d. 4 mm) fed with a 5 vol.% H_2/Ar purified carrier at the flow rate of 60 *STP* mL min^{-1}. The experiments were carried out in the range 273–1173 K with a heating rate of 20 K min^{-1}. The hydrogen consumption was monitored by a TCD, calibrated by the peak area of a known amount of CuO. TPR data resulted very reproducible both in maximum position (±3 K) and extent of H_2 consumption (±3%).

2.2.3. Transmission electron microscopy (TEM) analysis

TEM observations were made by using a *Philips CM12* instrument equipped with a high-resolution camera which allows acquisition and elaboration of the images. Specimens were prepared by ultrasonic dispersion of catalyst samples in isopropyl alcohol depositing a drop of suspension on holey carbon grid.

2.2.4. Ammonia temperature programmed desorption (NH_3-TPD)

NH_3-TPD measurements for the surface acidity determination were performed in a conventional flow apparatus by using 100 mg sample in a linear quartz micro-reactor (*internal diameter*, 4 mm; *length*, 200 mm), with a helium carrier flow rate of 25 *STP* mL min^{-1}. The experiments were carried out in the range 373–973 K with a heating rate of 10 K min^{-1}. The ammonia desorption was monitored by a thermal conductivity detector (TCD), calibrated by the peak area of known pulses of NH_3. Prior to each measurement, the sample was pretreated at 573 K with hydrogen flowing at 100 mL min^{-1} for 1 h and then cooled down to 423 K and saturated at a flow rate of 25 mL min^{-1} for 1.5 h with a 5% NH_3/He stream. Then, the samples were purged in He atmosphere for *ca.* 1 h until a constant TCD level was obtained.

2.3. Catalyst testing

The catalytic activity was investigated in a fixed-bed stainless steel reactor (*internal diameter*, 4 mm; *length*, 200 mm) at temperature ranging from 453 to 513 K and a total pressure of 3.0 MPa (F = 2.4 *STP* L/h; $CO_2/H_2/N_2$ = 3/9/1), using 0.25 g of hybrid catalyst (40–70 mesh), diluted with granular SiC (0.25 g). Prior to each test, the catalyst was reduced *in situ* at 573 K for 1 h in pure hydrogen flow at atmospheric pressure. The reaction stream was analyzed by a GC equipped with a two-column separation system connected to a *flame ionized detector* (FID) and *thermal conductivity detector* (TCD) respectively. Conversion values of CO_2 (X_{CO_2}) were calculated by both internal standard (a) and mass-balance (b) methods,

$$X_{CO_2} = 1 - \left[\left(\frac{CO_{2,out}}{CO_{2,in}}\right)\cdot\left(\frac{N_{2,in}}{N_{2,out}}\right)\right] \quad (a)$$

and

$$X_{CO_2} = \frac{CO_{2,out}}{\Sigma_{Pi}+CO_{2,out}}, \quad (b)$$

with product selectivity data (S_{Pi}) obtained from standard formulae:

$$S_{Pi} = \frac{P_i}{1 - CO_{2,out}} \quad (a')$$

and

$$S_{Pi} = \frac{P_i}{\Sigma_{P_i}} \quad (b')$$

where P_i stands for the concentration of a specific *i* product (*i.e.*, DME, MeOH, CO).

Each data set was obtained, with an accuracy of ±3%, from an average of three independent measurements.

3. Results and discussion

3.1. Textural properties

Table 1 shows the textural properties of the ZCZ and HZ30 components. The calcined ZCZ methanol synthesis catalyst displays a BET surface area of 173 $m^2\,g^{-1}$, which undergoes a significant shrinkage (*ca.* 54%) upon reduction treatment. Moreover, a decreasing pore volume before and after reduction (PV, 0.310–0.155 $cm^3\,g^{-1}$) mirrors a growth of the average pore diameter (APD) from 72 to 78 Å. On the other hand, typical BET and micropore volume values of 317 $m^2\,g^{-1}$ and 0.315 $cm^3\,g^{-1}$ were obtained for the HZ30 sample.

Being generally recognized that methanol forms directly from CO_2 and H_2 over a Cu single crystal with a very slow rate [52–54], the fundamental role of the metal/oxide interface, ensuring a suitable concentration of neighbouring hydrogenation and CO_2 activation sites, might be related to the promoting effect of both ZrO_2 and ZnO on the formation of the reaction intermediates *via* CO_2 adsorption [47–49]. Really, by an accurate TEM investigation of the reduced ZCZ system, it has been possible to discover that the core where the reaction occurs is mainly constituted by metallic copper Cu^0, decorated by Cu_2O, ZnO and ZrO_2, as clearly shown in Fig. 1, where the diffraction plane ⟨1 1 1⟩ corresponding to Cu_2O cuprite [JCPDS, 5-667], ⟨1 0 0⟩ relative to ZnO zincite syn hexagonal

Table 1
Main physico-chemical properties of the metallic (ZCZ) and acidic (HZ30) catalysts.

Sample	SA ($m^2\ g^{-1}$)		PV ($cm^3\ g^{-1}$)		APD[c] (Å)	
	Calcined	Reduced[b]	Calcined	Reduced[b]	Calcined	Reduced[b]
ZCZ[a]	173	80	0.310	0.155	72	78
HZ30	317	–	0.315	–	40	–

[a] Analytical composition (wt.%) of the fresh catalyst: CuO (41.2)/ZnO (14.8)/ZrO_2 (44.0) (see Ref. [50]).
[b] Sample reduced at 573 K (1 h) in flowing H_2 and then passivated at 293 K in a 2% O_2/He flow.
[c] Average pore diameter (APD, 4PV/SA).

Table 2
TPR data: onset temperature of reduction ($T_{o,red}$), temperature of peak maxima (T_{Mi}) and extent of hydrogen consumption.

Catalyst	$T_{o,red}$ (K)	$T_{1,max}$ (K)	$T_{2,max}$ (K)	H_2 uptake (mmol g_{ZCZ}^{-1})	H_2/Cu[a]
ZCZ	404	488	845	8.2	1.13
ZZ-G	397	489	853	7.0	1.03
ZZ-D	405	497	858	8.4	1.16
ZZ-M	411	515	853	7.2	1.06

[a] In the *T* range 273–573 K.

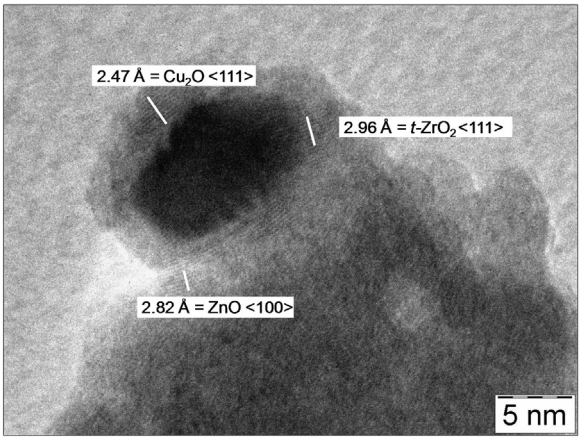

Fig. 1. TEM micrograph of the "reduced" ZCZ sample.

phase [JCPDS, 5-664] and ⟨1 1 1⟩ of ZrO_2 tetragonal phase [JCPDS, 17-923] are well distinguishable.

3.2. H_2-TPR

The reduction behaviour of the ZCZ functionality in the different hybrid catalysts was studied by H_2-TPR. The corresponding reduction profiles are shown in Fig. 2, while quantitative data are reported in Table 2, in terms of onset reduction temperature ($T_{o,red}$), temperature of peak maxima (T_{Mi}) and extent of hydrogen consumption.

All the ZCZ-containing systems display a similar reduction pattern, with a main peak centred between 488 and 515 K, accounting for the full reduction of CuO (H_2/Cu, 1.03–1.16), but at lower reduction temperature of bulk CuO. It is relevant that an easier reduction of CuO occurs for the ZZ-G sample (c), having a lower $T_{o,red}$ of 397 K, likely due to the preparation procedure of such a system that enhances the reactivity of the surface Cu^{2+} species. Furthermore, a baseline drift at $T > 573$ K, with a poorly pronounced maximum at 845–858 K, monitors the hard reduction of ZnO and/or decomposition of residual (hydroxyl)carbonate species coming from precursors [50] in a more or less strong extent of interaction with the acidic functions of the zeolite in the hybrid systems [46,55]. On the whole, an hydrogen consumption between 7.0 and 8.4 mmol g_{ZCZ}^{-1} does not allow to stress significant differences in terms of reducibility promoted by solid state interactions.

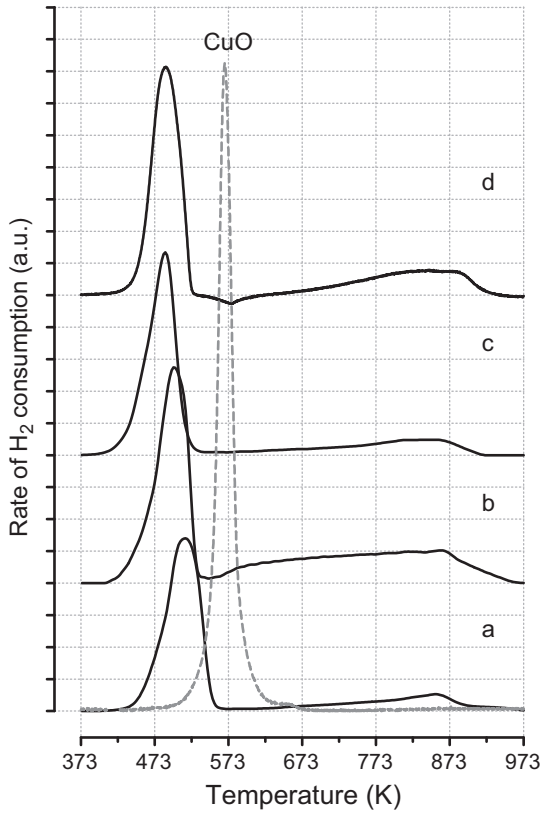

Fig. 2. TPR patterns of the studied catalytic samples: (a) ZZ-M; (b) ZZ-D; (c) ZZ-G and (d) ZCZ. Dashed profile refers to bulk CuO.

3.3. NH_3-TPD

It is generally recognized that ammonia is used as an excellent probe molecule for testing the acidic properties of solid catalysts. Thanks to its strong basicity and small molecular size, NH_3 allows the detection of acidic sites even located into very narrow pores [56].

The NH_3-TPD patterns of the investigated catalysts are shown in Fig. 3. Although the total acid amount can be more or less easily determined, the interpretation of the peak shape and position is often complicated by its dependence on the experimental conditions, like the amount of sample, activation and/or saturation treatments, as well as by kinetic phenomena (*e.g.*, re-adsorption,

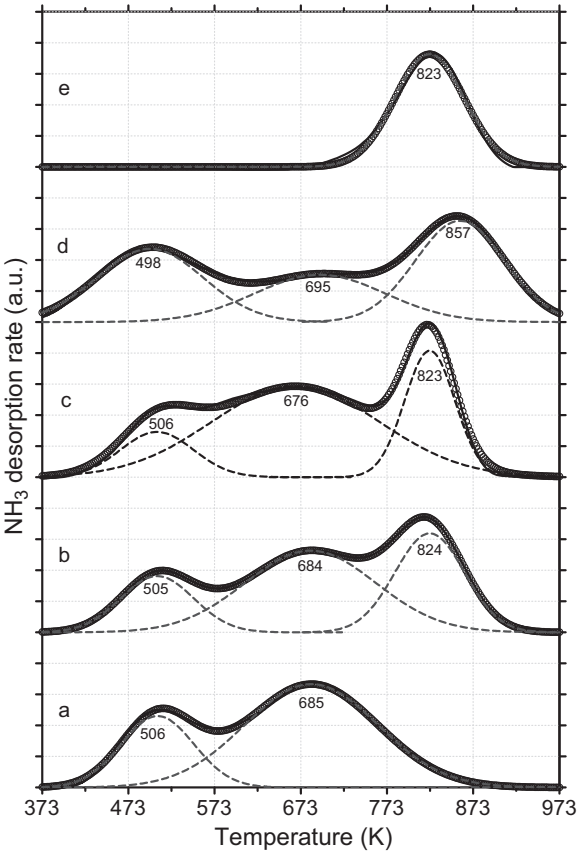

Fig. 3. NH_3-TPD deconvolution profiles: (a) HZ30; (b) ZZ-M; (c) ZZ-D; (d) ZZ-G and (e) ZCZ.

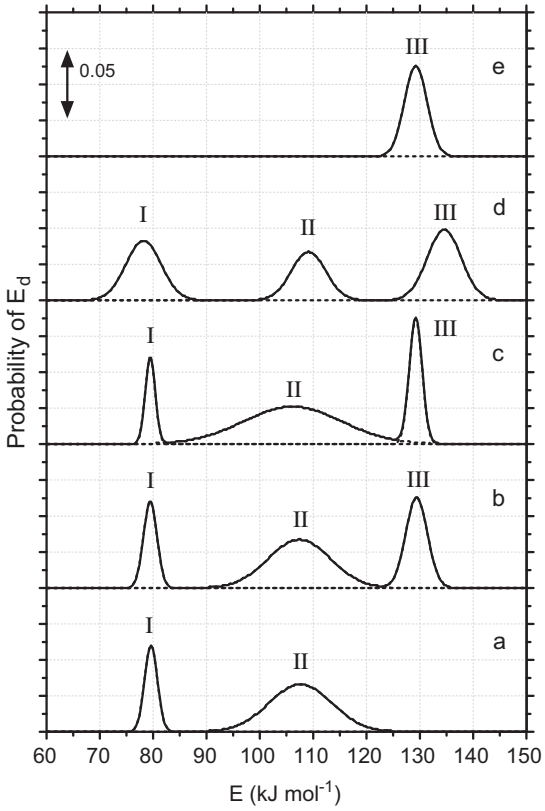

Fig. 4. Activation energy distribution of ammonia desorption: (a) HZ30; (b) ZZ-M; (c) ZZ-D; (d) ZZ-G and (e) ZCZ.

slow diffusion, etc.). Moreover, since the acid sites of comparable strength lead to overlapping peaks, only a mathematical analysis of the desorption pattern observed can allow to get insights on site distribution and heat of desorption [56–59].

As it is possible to observe, the HZ30 zeolite (a) shows two desorption peaks, indicating the existence of at least two types of acid sites: the first one (between 413 and 573 K) is normally attributed to the desorption of weakly bound ammonia. Really, the presence of these sites was found to be of scarce catalytic importance in DME production by methanol dehydration [60], but it is assumed that such sites could effectively influence the proton mobility in zeolites [61]. The second peak, in the temperature region between 573 and 813 K, appears prominent and it is usually attributed to the ammonia desorbed from the Brønsted acid sites [60,62].

The desorption profile of ZCZ methanol catalyst (e), instead, is characterized by one almost symmetric desorption peak, with the maximum at 823 K, accounting the desorption of about 0.38 mmol g_{cat}^{-1} of NH_3.

All the hybrid systems show similar desorption patterns, characterized by three peaks corresponding to the desorption of NH_3 from weak, medium and strong acid sites respectively. In particular, with a total adsorption capacity of 1.01 $mmol_{NH_3}$ g_{cat}^{-1}, the ZZ-M sample (b) outlines three resolved peaks centred at 505, 684 and 824 K, as a result of the contribution of the acid sites of zeolite (low and medium temperature) and ZCZ (high temperature).

Also, the ZZ-D sample (c) exhibits the predominance of medium and strong sites, with an overall population of *ca.* 86% and a lower concentration of weak sites. Moreover, such a sample bears a relatively higher coverage of NH_3 (1.20 mmol g_{cat}^{-1}), resulting almost equal to the sum of NH_3 desorbed from HZ30 and ZCZ samples respectively.

In spite of a similar shape of the desorption profile and a surface acidity of 1.06 mmol g_{cat}^{-1}, the ZZ-G sample (d) features a more balanced distribution of acid sites in the range of temperature investigated, with an evident shift of the maxima positions in respect of the other systems.

Such experimental NH_3-TPD profiles can be well fitted ($R^2 > 0.99$) with the contribution of three Gaussian functions, so allowing a reliable comparison of the acid properties, in terms of strength and concentration of sites. Moreover, considering the variety of surface sites involved in the adsorption processes, the distribution of the most probable activation energy related to the desorption of NH_3 from sites of different strength ($\bar{E}_{dn}$) can be also calculated. In fact, in the case of an energetically heterogeneous surface, the kinetic parameters (E, activation energy and A, pre-exponential factor) are not only a function of temperature, but also depend on the coverage degree [58]. Anyhow, according to Karge and Dondur [56], assuming first-order kinetics for the desorption rate and independent processes of NH_3 desorption from each site, the number of molecules remaining on the surface, as a function of time, depends on the probability density function. The energy distribution curves of the desorption patterns are presented in Fig. 4, on the basis of a constant pre-exponential factor ($A_{NH_3} = 2.5 \times 10^5\ s^{-1}$) derived from isothermal desorption experiments, while quantitative data are reported in Table 3.

Similar values of $\bar{E}_{dn}$ for each kind of sites (see Table 3) suggest that, under the adopted experimental conditions, the NH_3 desorption process is not significantly affected by diffusion limitations, accounting for weak ($\bar{E}_{d1} \approx 79$ kJ mol^{-1}), medium ($\bar{E}_{d2} \approx 107$ kJ mol^{-1}) and strong sites ($\bar{E}_{d3} \approx 130$ kJ mol^{-1}), that, as reported in literature, are in good agreement with strength of acidic sites of systems containing mordenites or zeolites [63–65]. Indeed, the shape of the Gaussian distributions in the hybrid systems (Fig. 4, patterns b–d) reveals the existence of two families of acid sites

Table 3
Analysis of NH_3-TPD patterns and acid sites distribution.[a]

Sample	Amount desorbed (mmol g_{cat}^{-1})	Weak sites				Medium sites				Strong sites			
		T_{d1} (K)	$\bar{E}_{d1}$ (kJ mol^{-1})	σ_1	x_1	T_{d2} (K)	$\bar{E}_{d2}$ (kJ mol^{-1})	σ_2	x_2	T_{d3} (K)	$\bar{E}_{d3}$ (kJ mol^{-1})	σ_3	x_3
ZCZ	0.38	–	–	–	–	–	–	–	–	823	129.2	2.1	1.00
ZZ-G	1.06	498	78.2	3.3	0.34	695	109.1	3.2	0.27	857	134.6	3.2	0.39
ZZ-D	1.20	506	79.5	0.9	0.14	676	106.2	9.2	0.60	823	129.2	1.2	0.26
ZZ-M	1.01	505	79.5	1.3	0.19	684	107.4	5.8	0.49	824	129.4	2.0	0.32
HZ30	0.88	506	79.6	1.2	0.27	685	107.6	5.9	0.73	–	–	–	–

[a] T_{dn}, temperature of desorption maximum; $\bar{E}_{dn}$ = most probable activation energy of desorption; σ_n, width of distribution; x_n, fractional population of sites.

belonging both to the zeolite (I, II) and the Cu–ZnO–ZrO_2 system (III). Usually, on sites of the same nature, the frequency of population (derivable by the width of peaks) of the first centre (I) tends to decrease much more rapidly than that of the second centre (II) and so on, as a consequence of a lower energy required for the desorption of a higher number of molecules chemisorbed at lower temperature. This concept results to be valid only for the first two Gaussian peaks (I, II) of ZZ-M (b) and ZZ-D (c), mirroring a desorption process from acid sites of the zeolite, while the narrow profile of the third peak (III) signals a population of acid sites different not only in strength but also in typology. Irrespective of the coverage of degree, a comparable width of distribution (see Table 3, σ_n = 3.2–3.3) related to the three types of acid sites (I–III) of the ZZ-G sample (d) clearly points out a sites re-distribution coming either from HZ30 or ZCZ systems, with a homogenization of the sites having different strength ($0.27 < x_n < 0.39$) and a shift of the NH_3 desorption energy, as a consequence of chemical interaction occurring during grinding in mortar to prepare a homogeneous system.

3.4. Thermodynamic evaluations

According to literature evidences, the main reactions involved in the global process of CO_2 hydrogenation to DME are summarized in Table 4. The corresponding equilibrium data calculated at 3.0 MPa are presented in Fig. 5. For the determination of equilibrium conversion of CO_2 and concentrations of components, reactions 1–3 have been selected as the independent processes, the reactions 4 and 5 being obtained from the linear combinations of the former ones. Apart from the Reverse Water Gas Shift reaction (RWGS, reaction 2), all the reactions are exothermic, resulting thermodynamically unfavoured with temperature increasing, as confirmed from the evaluation of K_p values in the temperature range of 453–513 K. Namely, it is evident a decreasing trend of CO_2 conversion (X_{CO_2}) in correspondence of a temperature increasing, with a maximum conversion value of 50% at 453 K becoming *ca.* 27% at 533 K. Within the investigated temperature range, the DME equilibrium selectivity gradually decreases from 83% to 54%, while a very small amount of CO forms below 493 K (<5%) that rapidly rises at higher temperature. Still, the effect of temperature appears less pronounced on the methanol production, since an almost constant selectivity from 15% to 19% is recorded between 453 and 533 K. Therefore, such findings imply that CO_2 hydrogenation reaction should be carried out at low temperature in order to maximize selectivity to DME.

3.5. Catalytic results

The comparison of the catalytic behaviour of the hybrid systems in the CO_2 hydrogenation reaction (P_R = 3.0 MPa; T_R = 453–513 K; GHSV = 10, 000 $NL\,kg_{cat}^{-1}\,h^{-1}$) is reported in Table 5, in terms of CO_2 conversion (X_{CO_2}) and product selectivity (S_x). No hydrocarbons or coke are formed under the adopted experimental conditions.

At 3.0 MPa and a space velocity high enough to limit mass-transfer constraints (see Fig. A in Supp. Info file), the hybrid systems show CO_2 conversion values rising from 1.6 (T = 453 K) to 16.1% (T = 513 K), counterbalanced by a parallel drop in S_{DME} from 70.9 to 33.9% and S_{CH3OH} from 21.7 to 11.8%, whereas S_{CO} drastically increases from 7.4% (453 K) to 54.3% (513 K). On the basis of thermodynamic data shown in Fig. 5, it can be seen that CO concentration is much higher than that expected from equilibrium. This behaviour clearly signals the occurrence of a full kinetic regime at any temperature investigated, where the ZZ-M sample explicates a superior performance, showing an improved CO_2 conversion trend in respect of the ZCZ methanol catalyst. Evidently, subtracting methanol from the equilibrium reaction, the incipient formation of DME promotes the conversion of CO_2. However, a decreasing trend of the ratio of $(S_{MeOH} + S_{DME})/S_{CO}$ with the temperature also confirms the faster reaction kinetics of the reverse water gas shift reaction [50].

In Fig. 6 the process productivity of the different studied systems, in the range of 453–513 K and 3.0 MPa is compared in terms of total methanol space-time yield (STY, $g_{total\,MeOH\,kg_{cat}^{-1}\,h^{-1}}$), considering the cumulative formation of methanol and DME. On the basis of such data, at 3.0 MPa the ZZ-M system features

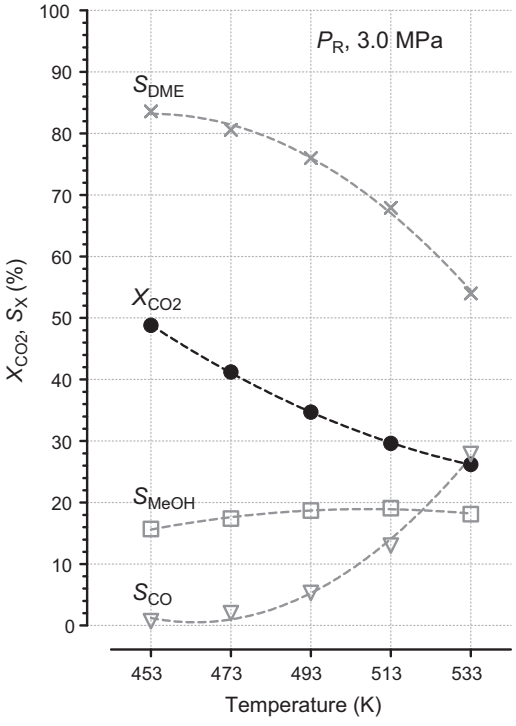

Fig. 5. Equilibrium values expected on the basis of thermodynamic analysis of direct DME synthesis from CO_2 hydrogenation (CO_2/H_2, 1/3 mol/mol).

Table 4
List of reactions involved in thermodynamics of the direct CO_2-to-DME synthesis.

Reaction	Stoichiometry	ΔH° (kJ mol^{-1})	K_P [a]			
			453 K	473 K	493 K	513 K
1	$CO_2 + 3H_2 \leftrightarrows CH_3OH + H_2O$	−49.4	2.95E−4	1.46E−4	7.64E−5	4.21E−5
2	$CO_2 + H_2 \leftrightarrows CO + H_2O$	+41.2	2.92E−3	4.54E−3	6.80E−3	9.86E−3
3	$2CH_3OH \leftrightarrows CH_3OCH_3 + H_2O$	−23.4	1.65E+1	1.42E+1	1.22E+1	1.06E+1
4	$CO + 2H_2 \leftrightarrows CH_3OH$	−90.6	1.01E−1	3.22E−2	1.12E−3	4.27E−3
5	$2CO_2 + 6H_2 \leftrightarrows CH_3OCH_3 + 3H_2O$	−122.2	1.44E−6	3.03E−7	7.12E−8	1.88E−8

[a] Equilibrium pressure constant with P_x values in MPa.

Table 5
Catalytic data (mol%) in the CO_2 hydrogenation reaction at different temperatures (P_R, 3.0 MPa; GHSV, 10, 000 $NL\,kg_{cat}^{-1}\,h^{-1}$; $CO_2/H_2/N_2$, 3/9/1).

Catalyst	T_R, 453 K				T_R, 473 K				T_R, 493 K				T_R, 513 K			
	X_{CO_2}	S_{DME}	S_{MeOH}	S_{CO}	X_{CO_2}	S_{DME}	S_{MeOH}	S_{CO}	X_{CO_2}	S_{DME}	S_{MeOH}	S_{CO}	X_{CO_2}	S_{DME}	S_{MeOH}	S_{CO}
ZCZ	1.5	–	100.0	0.0	3.5	–	86.8	13.2	6.6	–	71.8	28.2	10.5	–	53.8	46.2
ZZ-G	1.6	70.9	21.7	7.4	3.1	65.7	18.5	15.9	5.9	52.5	15.7	31.8	10.9	37.8	12.6	49.5
ZZ-D	1.9	75.3	16.6	8.1	4.1	66.3	16.2	17.5	8.3	51.5	13.8	34.6	13.8	36.6	11.0	52.4
ZZ-M	2.5	72.7	16.7	10.6	5.1	62.3	16.2	21.5	9.6	46.6	14.2	39.3	16.1	33.9	11.8	54.3

the best performance with STY values raising from 130 (453 K) to 430 $g_{total\,MeOH\,kg_{cat}^{-1}\,h^{-1}}$ (513 K). The ZZ-G system, instead, exhibits the lowest productivity with a maximum of *ca.* 300 $g_{total\,MeOH\,kg_{cat}^{-1}\,h^{-1}}$ at 513 K, while the ZZ-D sample attains STY values comparable with those of the ZCZ methanol catalyst. Namely, in the dual bed ZZ-D sample, MeOH formed in the initial step on ZCZ is converted into DME on acid sites in the second step, without any influence on the total methanol productivity. On the contrary, the effective mixing of the two catalytic systems in the ZZ-M sample results in a higher STY, in consequence of a higher conversion of CO_2 promoted by faster mass transfer phenomena occurring between neighbouring metal/oxide(s)-acid sites.The highest productivity obtained over the mixed catalyst (ZZ-M), with respect to the dual bed system configuration (ZZ-D), is attributable to an enhanced methanol mass transfer from the ZCZ catalyst sites to the zeolite acid sites: the closer the sites (metal/oxide and acid) the higher the rate conversion of methanol to DME, with positive consequences both in terms of thermodynamics (equilibrium shift with increased CO_2 conversion) and mass transfer phenomena.

On the basis of what previously inferred, by using the ZZ-G catalyst grinded in mortar, a better result was expected, due a more intimate contact between metal/oxide(s) and acid sites at interface. Really, the STY to total methanol obtained (Fig. 6) is much lower with respect to the other systems.

By TEM investigation (see Fig. 7) of reduced catalysts, it has been evidenced that grinding procedure determines a detrimental interaction between the two catalysts (ZCZ and H-ZSM5) due to a strong mechanical stress. This phenomenon causes a ZCZ structure destruction, so favouring the redistribution of metal copper ⟨2 0 0⟩ [JCPDS, 4-836] over zeolite (Fig. 7C) [1]. This should account for the loss of the catalytic activity of the hybrid ZZ-G catalyst.

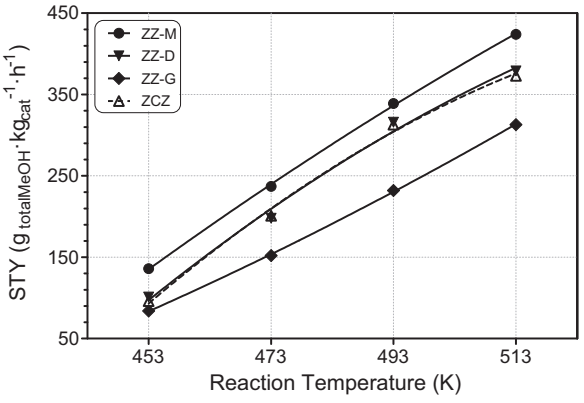

Fig. 6. Total MeOH productivity as a function of reaction temperature (GHSV, 10, 000 $NL\,kg_{cat}^{-1}\,h^{-1}$, P_R, 3.0 MPa).

Once defined that the best reactor configuration is ensured by the physical mixing of the catalysts, the influence of the optimal weight content of zeolite respect to ZCZ catalyst was investigated. The results are illustrated in Fig. 8, where the rate of CO_2 conversion and DME production, calculated for unit of methanol synthesis catalyst, is reported as a function of zeolite loading. No conversion of CO_2 was observed over the "bare" zeolite, because the lack of a specific functionality for CO_2 and H_2 activation. On the other hand, the rate of DME production in absence of zeolite results near to zero, although the strong acidity of the ZCZ system, as revealed by NH_3 adsorption measurements (see Fig. 5). This result clearly demonstrates that strong acid sites are not suitable to promote the dehydration reaction of methanol to DME. Overall, the rates of CO_2 conversion and DME production follow a volcano-shape trend with a maximum in correspondence of a HZ30 weight ratio of 0.5. This tendency is emphasized in the inset, where an "enhancement factor" (ε) of *ca.* 50% is reported as the ratio between the rate of CO_2 conversion on the hybrid system and on the ZCZ system. The result of Fig. 8 clearly shows that the catalytic behaviour of the combined system is highly dependent on the ratio of metal and acid surface sites. Only in the presence of an optimal ratio between such sites (ratio, 1/1 wt/wt) the equilibrium is shifted towards the formation of DME with consequent increase of the CO_2 conversion.

In Fig. 9, a further thermodynamic evaluation of the reactivity pattern of the ZZ-M sample, in terms of "β" parameters, corresponding to the ratio between the experimental K_{exp} constant (obtained from conversion-selectivity data) and the corresponding equilibrium K_{eq} constant (see Table 4) at that temperature is shown [50]. This analysis confirms that, apart from the methanol dehydration reaction (β_3), below 493 K all reaction paths proceed under a prevailing kinetic control. Only, being a fast reaction, the conversion of methanol to DME on the acid sites of the zeolite rapidly approaches the equilibrium level at any investigated temperature. The increasing trend of β_1 and β_2 values rising with the temperature suggests a parallel reaction network [50], although the lowest β_1 values indicate a poorer relative rate of MeOH synthesis in respect of CO formation. Moreover, based on β_1 and β_4 values, a promoting effect of the reaction temperature on the relative rate

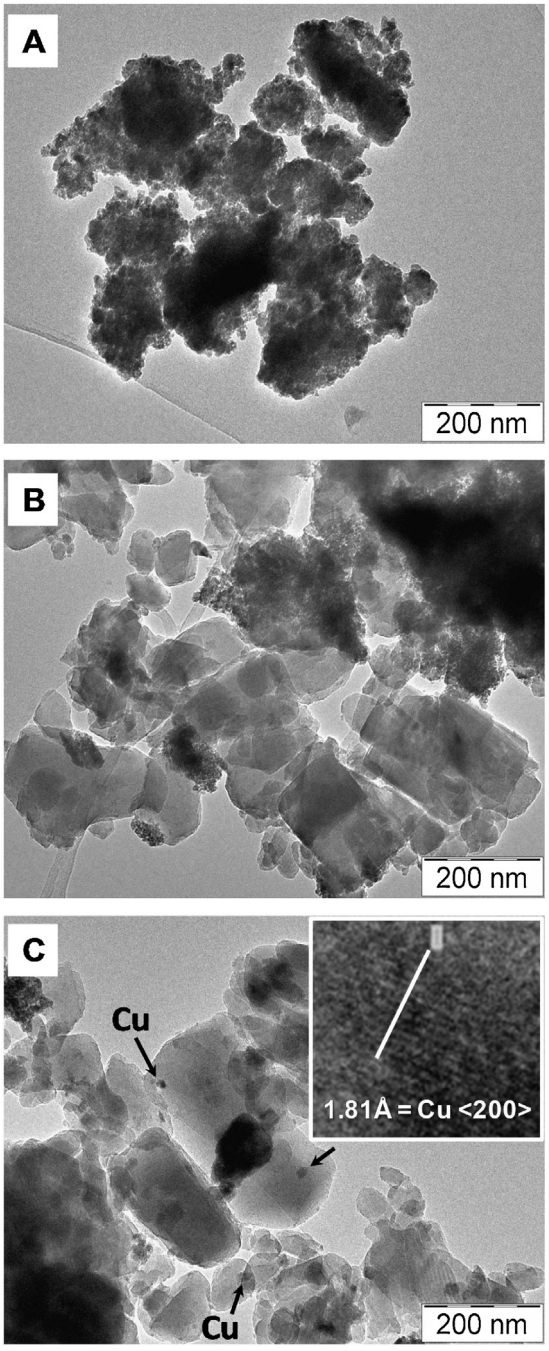

Fig. 7. TEM micrographs of the "reduced" ZCZ//HZ30 samples: (A) ZCZ; (B) ZZ-M; (C) ZZ-G.

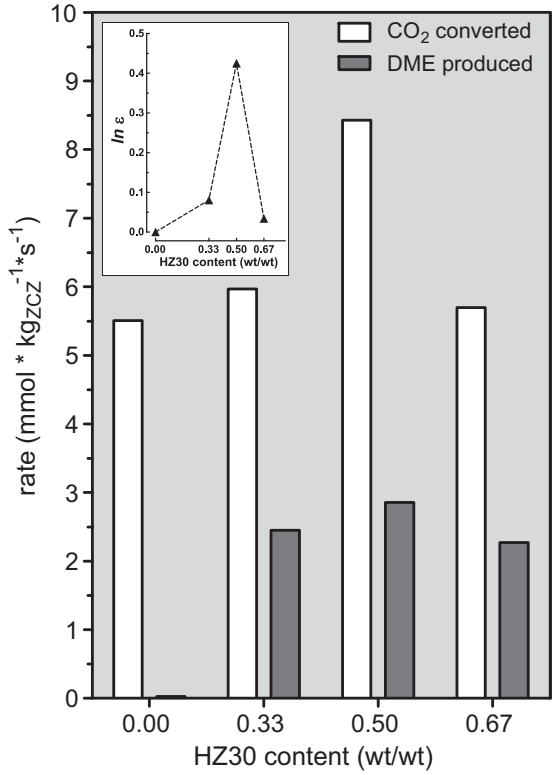

Fig. 8. Effect of the zeolite content on the reaction rate (T_R, 513 K; P_R, 3.0 MPa; GHSV, 10, 000 $NL\,kg_{cat}^{-1}\,h^{-1}$). In the inset, the enhancement factor (ε) of CO_2 conversion is reported.

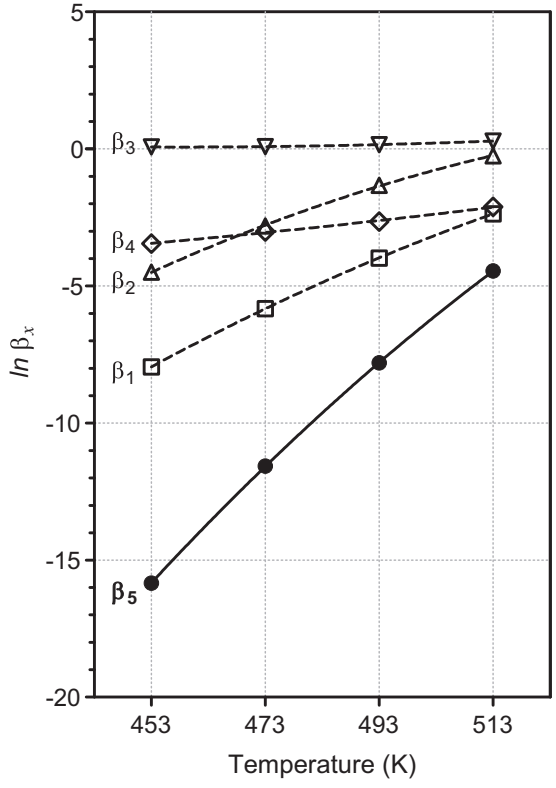

Fig. 9. CO_2 hydrogenation reaction (P_R, 3.0 MPa; GHSV, 10, 000 $NL\,kg_{cat}^{-1}\,h^{-1}$). Ratio ($\beta$) between experimental and theoretical equilibrium constants (K_P) of CO_2 hydrogenation to methanol (β_1), reverse water gas shift (β_2), methanol dehydration to DME (β_3), CO hydrogenation to methanol (β_4) and direct synthesis of DME from CO_2 (β_5) *vs.* reaction temperature (K).

of methanol synthesis from CO_2 rather than CO is observed, as also expected on the basis of thermodynamics. Still, at $T_R > 473$ K, β_2 overcomes β_4 values until reaching the equilibrium state at 513 K, so explaining the relevant CO selectivity values obtained at high temperature.

On the whole, according to the reaction scheme proposed in Fig. 10, such findings prove that, apart from the reaction 3 that takes place very fast at any temperature, reactions 1-2-4 affect the methanol formation in dependence of their relative reaction rates which significantly change with temperature. In particular, at a temperature as low as 453 K, MeOH synthesis prevails on CO formation ($\beta_2 < \beta_4$), whereas at higher temperature this trend appears inverted ($\beta_2 > \beta_4$), although a progressive improvement in β_1 is also observed. Then, since CO is inevitably produced during

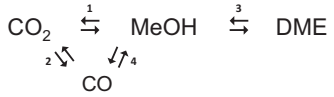

Fig. 10. Reaction scheme comprising the paths involved in the direct CO_2 hydrogenation to DME. Numbers refer to the reaction described in Table 4.

DME production in the one-step CO_2 hydrogenation reaction, operation at low temperature with an effective recycle of CO_x/H_2 stream could result in an enhanced catalyst productivity.

4. Conclusions

The catalytic behaviour of a hybrid Cu–ZnO–ZrO_2/H-ZSM5 system in the one-step DME synthesis by CO_2 hydrogenation reaction has been assessed.

Among the investigated catalysts, the hybrid system Cu–ZnO–ZrO_2/H-ZSM5, prepared by physical mixing of pre-pelletized samples, exhibits a superior performance in the direct CO_2 conversion to DME giving at 3.0 MPa and 513 K a specific productivity of *ca.* 430 $g_{\text{total MeOH}}\, kg_{\text{cat}}^{-1}\, h^{-1}$ under a full kinetic regime. Set-up of two sequential catalytic beds (Cu–ZnO–ZrO_2 and H-ZSM5) within the same reactor does not produce any advantage in respect of a single bed of Cu–ZnO–ZrO_2 in terms of total methanol yield, due to thermodynamic constraints relating to methanol synthesis from CO_2. Moreover, the poor performance of the hybrid catalyst prepared by grinding of active components in mortar is explained in the light of a complete destruction of the system, during mortar treatment, as demonstrated by a re-distribution of active sites on the surface.

Catalytic data in absence of zeolite disclose that strong acid sites of the methanol catalyst are not suitable to produce DME at significant reaction rate, while a higher CO_2 conversion rate is obtained when an optimal ratio of 1:1 (wt/wt) between methanol synthesis catalyst and zeolite is used to prepare a hybrid catalyst. This demonstrates that an ideal bifunctional catalyst should contain a balanced concentration of metal/oxide(s) and weak-medium acid sites.

The thermodynamic analysis of the main reaction paths involved in the synthesis of DME by CO_2 hydrogenation reveals that, under kinetic conditions, CO concentration dramatically increases with temperature; therefore, low reaction temperature and recycling unreacted CO_x/H_2 mixture could be a solution to improve the methanol/DME productivity.

Acknowledgements

Dr. Gaetano Maggio and Dr. Giosuè Giacoppo are gratefully acknowledged for their contribution in solving non linear equation group of the independent reactions selected for equilibrium data calculations of the direct CO_2 hydrogenation reaction to DME by implementation of Gauss-Newton arithmetic in the MATHCAD programme.

Appendix A.

Supporting Info file related to this paper can be found in the online version.

Appendix B. Supplementary data

Supplementary data associated with this article can be found, in the online version, at http://dx.doi.org/10.1016/j.apcatb.2013.03.048.

References

[1] A. García-Trenco, A. Vidal-Moya, A. Martínez, Catalysis Today 179 (2012) 43–51.
[2] N. Tsubaki, M. Ito, K. Fujimoto, Journal of Catalysis 197 (2001) 224–227.
[3] T. Sakakura, K. Kohno, Chemical Communications (2009) 1312–1330.
[4] M. Mikkelsen, M. Jørgensen, F.C. Krebs, Energy Environmental Science 3 (2010) 43–81.
[5] W. Wang, S. Wang, X. Ma, J. Gong, Chemical Society Reviews 40 (2011) 3703–3727.
[6] T.A. Semelsberger, K.C. Ott, R.L. Borup, H.L. Greene, Applied Catalysis A 309 (2006) 210–223.
[7] M. Nilsson, L.J. Pettersson, B. Lindstrom, Energy and Fuels 20 (2006) 2164–2169.
[8] V.M. Lebarbier, R.A. Dagle, L. Kovarik, J.A. Lizarazo-Adarme, D.L. King, D.R. Palo, Catalysis Science and Technology 2 (2012) 2116–2127.
[9] J.W. Jung, Y.J. Lee, S.H. Um, P.J. Yoo, D.H. Lee, K.-W. Jun, J.W. Bae, Applied Catalysis B 126 (2012) 1–8.
[10] A. García-Trenco, A. Martínez, Applied Catalysis A 411–412 (2012) 170–179.
[11] J.H. Flores, D.P.B. Peixoto, L.G. Appel, R.R. De Avillez, M.I.P.D. Silva, Catalysis Today 172 (2011) 218–225.
[12] S.-C. Baek, S.-H. Kang, J.W. Bae, Y.-J. Lee, D.-H. Lee, K.-Y. Lee, Energy and Fuels 25 (2011) 2438–2443.
[13] Y. Luan, Advanced Materials Research 183–185 (2011) 1505–1508.
[14] J. Palgunadi, I. Yati, K.D. Jung, Reaction Kinetics, Mechanisms and Catalysis 101 (2010) 117–128.
[15] P.S.S. Prasad, J.W. Bae, S.H. Kang, Y.J. Lee, K.W. Jun, Fuel Processing Technology 89 (2008) 1281–1286.
[16] S.H. Kang, J.W. Bae, K.W. Jun, H.S. Potdar, Catalysis Communications 9 (2008) 2035–2039.
[17] K.S. Yoo, J.H. Kim, M.J. Park, S.J. Kim, O.S. Joo, K.D. Jung, Applied Catalysis A 330 (2007) 57–62.
[18] F.S. Ramos, A.M. Duarte de Farias, L.E.P. Borges, J.L. Monteiro, M.A. Fraga, E.F. Sousa-Aguiar, L.G. Appel, Catalysis Today 101 (2005) 39–44.
[19] K. Sun, W. Lu, F. Qiu, S. Liu, X. Xu, Applied Catalysis A 252 (2003) 243–249.
[20] Q. Zhang, Y.-Z. Zuo, M.-H. Han, J.-F. Wang, Y. Jin, F. Wei, Catalysis Today 150 (2010) 55–60.
[21] S. Wang, D. Mao, X. Guo, G. Wu, G. Lu, Catalysis Communications 10 (2009) 1367–1370.
[22] X. An, Y.Z. Zuo, Q. Zhang, D.Z. Wang, J.F. Wang, Industrial and Engineering Chemistry Research 47 (2008) 6547–6554.
[23] J.-Y. Wang, X.-H. Wang, C.-Y. Zeng, C.-Z. Wu, S. Xuebao, S. Jiagong, Acta Petrolei Sinica (Petroleum Processing Section) 23 (2007) 62–68.
[24] J.-Y. Wang, C.-Y. Zeng, C.-Z. Wu, Journal of Fuel Chemistry and Technology 34 (2006) 195–199.
[25] J.-Y. Wang, C.-Y. Zeng, X. Huagong, Modern Chemical Industry 26 (2006) 35–39.
[26] H.-W. Liu, D.-H. Liu, W.-Y. Ying, D.-Y. Fang, G. Huaxue, G. Xuebao, Journal of Chemical Engineering of Chinese Universities 19 (2005) 59–64.
[27] F. Arena, L. Spadaro, O. Di Blasi, G. Bonura, F. Frusteri, Studies in Surface Science and Catalysis 147 (2004) 385–390.
[28] K. Sun, W. Lu, M. Wang, X. Xu, Catalysis Communications 5 (2004) 367–370.
[29] T. Tagawa, M. Ito, S. Goto, Applied Organometallic Chemistry 15 (2001) 105–108.
[30] S.P. Naik, T. Ryu, V. Bui, J.D. Miller, N.B. Drinnan, W. Zmierczak, Chemical Engineering Journal 167 (2011) 362–368.
[31] J. Ereña, I. Sierra, A.T. Aguayo, A. Ateka, M. Olazar, J. Bilbao, Chemical Engineering Journal 174 (2011) 660–667.
[32] Y. Zhao, J. Chen, J. Zhang, Journal of Natural Gas Chemistry 16 (2007) 389–392.
[33] G.R. Moradi, S. Nosrati, F. Yaripor, Catalysis Communications 8 (2007) 598–606.
[34] D. Mao, W. Yang, J. Xia, B. Zhang, G. Lu, Journal of Molecular Catalysis A-Chemical 250 (2006) 138–144.
[35] F. Yaripour, F. Baghaei, I. Schmidt, J. Perregaard, Catalysis Communications 6 (2005) 147–152.
[36] T. Takeguchi, K. Yanagisawa, T. Inui, M. Inoue, Applied Catalysis A 192 (2000) 201–209.
[37] J.L. Li, X.G. Zhang, T. Inui, Applied Catalysis A 147 (1996) 23–33.
[38] G. Laugel, X. Nitsch, F. Ocampo, B. Louis, Applied Catalysis A 402 (2011) 139–145.
[39] S. Ivanova, C. Lebrun, E. Vanhaecke, C. Pham-Huu, B. Louis, Journal of Catalysis 265 (2009) 1–7.
[40] L. Wang, Y. Qi, Y. Wei, D. Fang, S. Meng, Z. Liu, Catalysis Letters 106 (2006) 61–66.
[41] J. Ereña, R. Garoña, J.M. Arandes, A.T. Aguayo, J. Bilbao, Catalysis Today 107–108 (2005) 467–473.
[42] D. Mao, W. Yang, J. Xia, B. Zhang, Q. Song, Q. Chen, Journal of Catalysis 230 (2005) 140–149.
[43] J.H. Kim, M.J. Park, S.J. Kim, O.S. Joo, K.D. Jung, Applied Catalysis A 264 (2004) 37–41.
[44] V. Vishwanathan, K.-W. Jun, J.-W. Kim, H.-S. Roh, Applied Catalysis A 276 (2004) 251–255.
[45] J. Xia, D. Mao, B. Zhang, Q. Chen, Y. Tang, Catalysis Letters 98 (2004) 235–240.
[46] Q. Ge, Y. Huang, F. Qiu, S. Li, Applied Catalysis A 167 (1998) 23–30.
[47] G. Bonura, F. Arena, G. Mezzatesta, C. Cannilla, L. Spadaro, F. Frusteri, Catalysis Today 171 (2011) 251–256.
[48] F. Arena, G. Italiano, K. Barbera, G. Bonura, L. Spadaro, F. Frusteri, Catalysis Today 143 (2009) 80–85.

[49] F. Arena, G. Italiano, K. Barbera, S. Bordiga, G. Bonura, L. Spadaro, F. Frusteri, Applied Catalysis A 350 (2008) 16–23.
[50] F. Arena, K. Barbera, G. Italiano, G. Bonura, L. Spadaro, F. Frusteri, Journal of Catalysis 249 (2007) 183–192.
[51] M. Xu, J.H. Lunsford, D.W. Goodman, A. Bhattacharyya, Applied Catalysis A 149 (1997) 289–301.
[52] T. Fujitani, J. Nakamura, Applied Catalysis A 191 (2000) 111–129.
[53] P.B. Rasmussen, P.M. Holmblad, T. Askgaard, C.V. Ovesen, P. Soltze, J.K. Nørskov, I. Chorkendorff, Catalysis Letters 26 (1994) 373–381.
[54] P.B. Rasmussen, M. Kazuta, I. Chorkendorff, Surface Science 318 (1994) 267–280.
[55] G.R. Moradi, M. Nazari, F. Yaripour, Fuel Processing Technology 89 (2008) 1287–1296.
[56] H.G. Karge, V. Dondur, Journal of Physical Chemistry 94 (1990) 765–772.
[57] P. Redhead, Vaccine 12 (1962) 203–211.
[58] V. Dondur, D. Fidler, Surface Science 150 (1985) 480–486.
[59] F. Arena, R. Dario, A. Parmaliana, Applied Catalysis A 170 (1998) 127–137.
[60] M. Niwa, N. Katada, Catalysis Surveys from Japan 1 (1997) 215–226.
[61] L. Rodríguez-González, F. Hermes, M. Bertmer, E. Rodríguez-Castellón, A. Jiménez-López, U. Simon, Applied Catalysis A 328 (2007) 174–182.
[62] N. Katada, H. Igi, J. Kim, M. Niwa, Journal of Physical Chemistry B 110 (1997) 5969–5997.
[63] M.C. Abello, A.P. Velasco, M.F. Gomez, J.B. Rivarola, Langmuir 13 (1997) 2596–2599.
[64] D. Li, F. Li, J. Ren, Y. Sun, Applied Catalysis A 241 (2003) 15–24.
[65] F. Lónyi, J. Valyon, Microporous and Mesoporous Materials 47 (2001) 293–301.